nature neuroscience

Cholinergic modulation of multivesicular release regulates striatal synaptic potency and integration

Michael J Higley[1,2], Gilberto J Soler-Llavina[1,2] & Bernardo L Sabatini[1]

The pleiotropic actions of neuromodulators on pre- and postsynaptic targets make disentangling the mechanisms underlying regulation of synaptic transmission challenging. In the striatum, acetylcholine modulates glutamate release via activation of muscarinic receptors (mAchRs), although the consequences for postsynaptic signaling are unclear. Using two-photon microscopy and glutamate uncaging to examine individual synapses in the rat striatum, we found that glutamatergic afferents have a high degree of multivesicular release (MVR) in the absence of postsynaptic receptor saturation. We found that mAchR activation decreased both the probability of release and the concentration of glutamate in the synaptic cleft. The corresponding decrease in synaptic potency reduced the duration of synaptic potentials and limited temporal summation of afferent inputs. These findings reveal a mechanism by which a combination of basal MVR and low receptor saturation allow the presynaptic actions of a neuromodulator to control the engagement of postsynaptic nonlinearities and regulate synaptic integration.

Neuromodulatory systems in the mammalian brain regulate behavioral state, circuit plasticity and synaptic transmission[1]. Perturbations of neuromodulators such as acetylcholine (Ach), dopamine and serotonin contribute to the pathogenesis and treatment of neuropsychiatric disorders including Parkinson's disease, schizophrenia and major depression[2–5]. In contrast with classical neurotransmitters that directly excite or inhibit postsynaptic neurons, neuromodulators generally alter the biochemical state of the neuron, influencing the activities of receptors, ion channels and signaling cascades. These pleiotropic effects present major technical challenges to the elucidation of the specific mechanisms underlying neuromodulation of brain function. This difficulty is evident in the striatum, an important component of the basal ganglia that is necessary for the proper generation of movement and that is regulated by neuromodulators such as dopamine and Ach[6–8]. Ach is released in the striatum by interneurons, and disruption of cholinergic signaling impairs both movement and learning of operant conditioning tasks[9,10]. Moreover, perturbation of striatal cholinergic signaling contributes to movement disorders that include Huntington's and Parkinson's diseases[4,11,12].

The majority of cells in the striatum are medium spiny neurons (MSNs) that receive glutamatergic inputs from the cortex and thalamus[13,14]. Presynaptic terminals of these afferents express M2-type mAchRs, whose activation reduces the magnitude of synaptic responses in the striatum[15–19]. MSNs express both M1- and M4-type mAchRs, and ultrastructural analysis has shown that cholinergic terminals are typically apposed to dendritic shafts and spine necks, suggesting that cholinergic receptors may also regulate postsynaptic properties[20–22]. Previous studies found minimal effects of mAchR activation on postsynaptic glutamatergic currents[16,23] (but see ref. 24). Nevertheless, mAchR activation modulates the intrinsic membrane properties of MSNs, reducing currents through various voltage-gated Ca^{2+} and K^+ channels[25–28]. As nonlinear interactions between voltage-sensitive glutamate receptors and other channels can influence synaptic response magnitude and integration[29,30], muscarinic actions on glutamatergic signaling remain unclear.

We studied the modulation of excitatory synapses onto MSNs, combining two-photon laser-scanning microscopy (2PLSM) and two-photon laser uncaging of glutamate (2PLU) to determine the pre- and postsynaptic actions of mAchRs. Optical quantal analysis revealed that mAchR activation reduced both the probability of glutamate release from the presynaptic terminal and the potency of individual synapses. However, mAchR activation did not directly modulate glutamate receptors. Our results indicate that striatal glutamatergic synapses exhibit a high basal rate of MVR without substantial saturation of glutamate receptors. We found that synaptic potency regulated the duration and temporal summation of excitatory postsynaptic potentials. Thus, the combination of basal MVR, lack of receptor saturation and dendritic nonlinearities allows presynaptic neuromodulation to control both synaptic potency and temporal integration in MSNs.

RESULTS

We measured the effects of mAchR activation on glutamatergic postsynaptic responses in the striatum. In whole-cell current-clamp recordings, paired-pulse electrical stimulation (50-ms interval) evoked depressing excitatory postsynaptic potentials (EPSPs; **Fig. 1a**). Application of muscarine, a general mAchR agonist, reduced the amplitudes of evoked responses, depolarized the resting membrane potential

[1]Howard Hughes Medical Institute, Department of Neurobiology, Harvard Medical School, Boston, Massachusetts, USA. [2]These authors contributed equally to this work. Correspondence should be addressed to B.L.S. (bsabatini@hms.harvard.edu).

Received 14 May; accepted 11 June; published online 9 August 2009; doi:10.1038/nn.2368

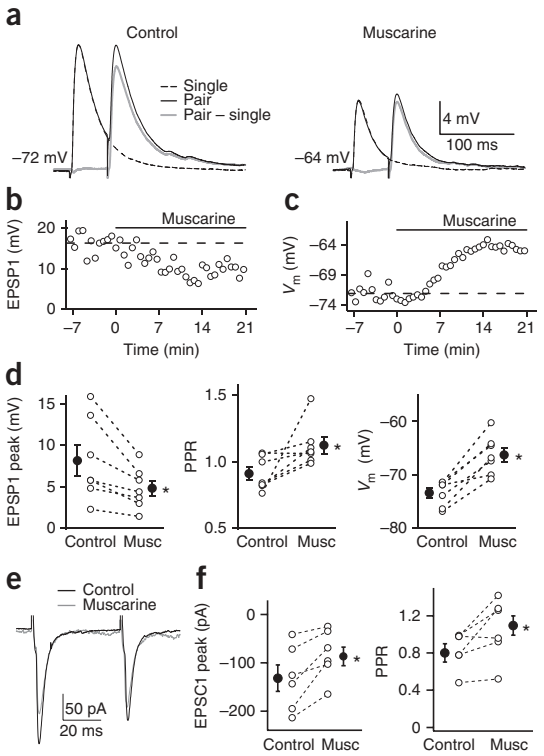

(V_m; **Fig. 1a–c**) and increased the paired-pulse ratio (PPR). On average ($n = 7$), muscarine reduced the first EPSP from 8.1 ± 1.6 mV to 4.8 ± 0.8 mV ($P < 0.05$) and the second EPSP from 6.5 ± 1.4 mV to 4.9 ± 0.8 mV ($P < 0.05$), increasing the PPR from 0.9 ± 0.1 to 1.2 ± 0.1 ($P < 0.05$) (**Fig. 1d**). The average V_m depolarized from −73.6 ± 0.8 mV to −67.8 ± 1.6 mV ($P < 0.05$; **Fig. 1d**), without change in the input resistance (data not shown). In whole-cell voltage-clamp recordings ($V_{hold} = -75$ mV), muscarine reduced the amplitudes of excitatory postsynaptic currents (EPSCs) and increased the PPR (**Fig. 1e**). On average ($n = 6$), muscarine reduced the first EPSC from 131.8 ± 27.5 pA to 86.7 ± 19.3 pA ($P < 0.05$) and the second EPSC from 111.7 ± 26.2 pA to 89.9 ± 20.7 pA ($P < 0.05$), increasing the PPR from 0.8 ± 0.1 to 1.1 ± 0.1 ($P < 0.05$; **Fig. 1f**). These data indicate that mAchR activation exerts both presynaptic (alterations in PPR) and postsynaptic (depolarization) actions in addition to producing effects of unclear origin (reduction of synaptic responses).

Figure 1 Modulation of synaptic responses and passive properties of MSNs by mAchRs. (**a**) Left, single (dashed line) and paired (solid, black line) EPSPs recorded from a MSN under control conditions. The difference between the paired and single EPSP is shown (gray). Right, EPSPs recorded after the addition of 10 μM muscarine. EPSPs are averages of 10 consecutive trials. (**b**) Time course of the first EPSP (EPSP1) amplitude from the experiment shown in **a**. Muscarine was applied during the time indicated by the horizontal bar. (**c**) Time course of the V_m from the experiment shown in **a**. (**d**) EPSP1 peak amplitude (left), PPR (middle) and V_m (right) for each recorded cell (open circles) in control conditions and after the addition of muscarine (musc). Mean values ± s.e.m. are shown (closed circles). (**e**) Paired EPSCs recorded from a MSN under voltage clamp (holding potential was −75 mV) before (black line) and after (gray line) application of muscarine. (**f**) EPSC1 peak amplitude (left) and PPR (right) for each recorded cell (open circles) before and after muscarine addition. Mean values ± s.e.m. are shown (closed circles). * indicates a significant difference between groups ($P < 0.05$).

Optical quantal analysis of glutamatergic synapses

To determine the effects of mAchR activation at individual synapses, we measured the probability of vesicular release and the synaptic potency (the average response magnitude when release occurs from the presynaptic terminal[31,32]) with optical quantal analysis. 2PLSM was used to place a stimulating electrode ~10 μm from spiny regions of the proximal dendrite (**Fig. 2a**). Electrode position and stimulus strength were adjusted until a single spine in the field of view was activated, as judged by a Ca^{2+}-dependent increase in green fluorescence limited to a single spine head (**Fig. 2b**). Recordings were made in the presence of the AMPA receptor (AMPAR) antagonist 2,3-dihydroxy-6-nitro-7-sulfamoyl-benzo[f]quinoxaline-2,3-dione (NBQX) and the cell was voltage-clamped at 0–10 mV (the empirically determined reversal potential for NMDA receptors, NMDARs) to eliminate net synaptically evoked current and prevent changes in potential in the active spine. By collecting evoked fluorescence changes in the spine and neighboring dendrite, success and failure trials could be distinguished (**Fig. 2c**). Under these conditions, synaptic Ca^{2+} influx

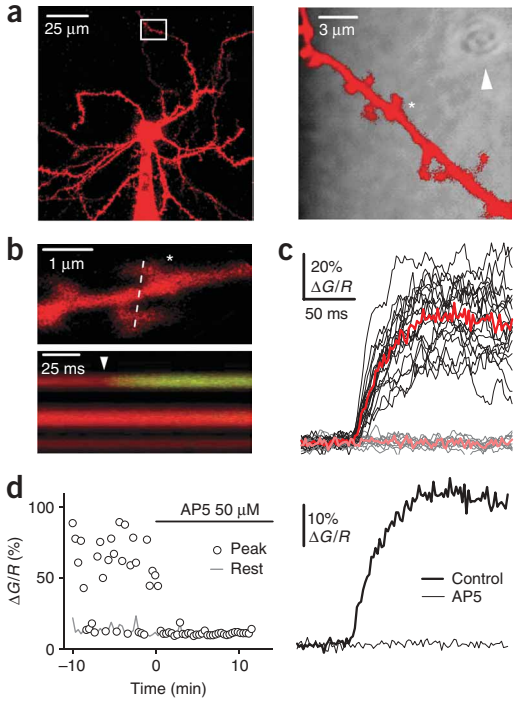

Figure 2 Optical quantal analysis of synaptic potency and failure rate. (**a**) Left, 2PLSM image of an MSN filled with 20 μM Alexa-594 and 300 μM Fluo-5F. Right, higher-magnification image of the boxed region. The segment of dendrite is shown overlaid on a laser-scanning differential interference contrast image of the slice. The extracellular stimulating electrode (arrowhead) is located near a spine containing an activated synapse (*). (**b**) Top, enlarged image of the dendrite shown in **a**. Bottom, fluorescence collected in a line scan as indicated by the dashed line in the top panel during electrically evoked synaptic activation. The image is an average of 19 successful trials. The stimulus evoked a Ca^{2+} transient that was limited to the upper (*) spine. (**c**) Quantification of synaptically evoked fluorescence transients ($\Delta G/R$) in the active spine showing successes (black) and failures (gray) of synaptic transmission. The red and pink traces are the averages of the black and gray traces, respectively. (**d**) Left, time course of the peak $\Delta G/R$ (circles) and resting fluorescence (gray line) during a 10-min baseline period and after application of the NMDAR antagonist AP5 (50 μM). The baseline period of this time course corresponds to the traces shown in **c**. Right, average of 30 consecutive trials (successes and failures) during the baseline (thick line) and in the presence of AP5 (thin line).

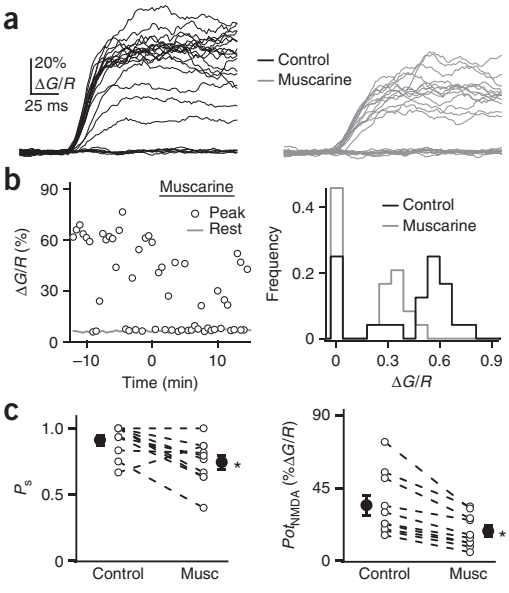

Figure 3 mAchR activation increases synaptic failures and decreases NMDAR-mediated synaptic potency. (**a**) Left, $\Delta G/R$ from a representative spine in control ACSF showing synaptic successes and failures. Right, $\Delta G/R$ in the same spine after bath application of muscarine (10 μM). (**b**) Left, time course of the peak $\Delta G/R$ (circles) and resting fluorescence (gray line) during a baseline period and after application of muscarine. Right, corresponding histogram of $\Delta G/R$ amplitudes in the two conditions. (**c**) Probability of success (P_s, left) and synaptic potency (Pot_{NMDA}, right) for each spine (open circles) under control conditions and after the addition of muscarine (musc). Mean values ± s.e.m. are shown (closed circles). * indicates a significant difference between groups ($P < 0.05$).

occurred through NMDARs and was blocked by the NMDAR antagonist D(−)-2-amino-5-phosphonovaleric acid (AP5; **Fig. 2d**). The probability of success of glutamate release (P_s) was determined as the fraction of trials that evoked a fluorescence transient in the spine head. Synaptic potency (Pot_{NMDA}) was measured as the average amplitude of fluorescence transients in the spine head ($\Delta G/R$) in successful trials.

In a separate set of experiments, we monitored P_s and Pot_{NMDA} in individual spines during application of muscarine (**Fig. 3a**). Muscarine increased the fraction of failure trials and decreased $\Delta G/R$ on success trials with no effect on resting fluorescence (**Fig. 3b**). On average ($n = 10$), muscarine decreased P_s from 0.91 ± 0.04 to 0.74 ± 0.05 ($P < 0.05$) and Pot_{NMDA} from 34.3 ± 6.1% to 18.4 ± 3.2% ($P < 0.05$; **Fig. 3c**).

Uncaging-evoked synaptic currents and Ca^{2+} transients

To determine whether mAchRs directly regulate postsynaptic glutamate receptors, we examined responses evoked by 2PLU. MSNs were voltage-clamped at −70 mV in the presence of tetrodotoxin (TTX) and voltage-gated calcium channel (VGCC) blockers (see Online Methods). To stimulate each spine with a consistent amount of glutamate, we adjusted the laser power such that a 500-μs pulse directed at the spine head bleached ~50% of the red fluorescence (**Fig. 4a–c**)[33]. After setting laser power, the periphery of the spine was probed to find the uncaging position that evoked the largest uncaging-evoked EPSC (uEPSC)[34]. In the presence of the NMDAR antagonist (RS)-3-(2-carboxypiperazin-4-yl)-propyl-1-phosphonic acid (CPP), uncaging evoked brief inward currents (**Fig. 4d**) with amplitudes similar to those of miniature EPSCs[35]. On average ($n = 26$), the non-NMDAR-mediated uEPSC was 17.2 ± 1.6 pA (**Fig. 4e**) and was not significantly altered in the presence of muscarine (17.4 ± 2.4 pA, $n = 24$, $P > 0.05$), indicating that mAchR activation does not modulate postsynaptic AMPAR currents.

We performed a similar analysis in the presence of the AMPAR antagonist NBQX and in nominally 0 mM extracellular Mg^{2+}. In these conditions, at a holding potential of −70 mV, 2PLU evoked NMDAR-mediated uEPSCs and Ca^{2+} influx into the spine (**Fig. 5a–d**). Neither NMDAR-mediated currents nor Ca influx under control conditions (5.0 ± 0.7 pA, $\Delta G/R = 46.0 \pm 6.1\%$, $n = 15$) were significantly different from those that occurred in the presence of muscarine (4.3 ± 0.6 pA, $\Delta G/R = 49.2 \pm 6.3\%$, $n = 15$, $P > 0.05$; **Fig. 5e**). When we repeated these experiments under the voltage-clamp conditions that we used for optical quantal analysis (0–10 mV), there was negligible NMDAR-mediated current flow and muscarine again had no effect on NMDAR-mediated Ca^{2+} transients ($n = 19$, $\Delta G/R = 195.4 \pm 19.2\%$ versus 200.7 ± 27.4% for control and muscarine, respectively; **Fig. 5f**). Thus, although activation of mAchRs regulates NMDAR-mediated synaptic potency, it does not directly modulate the opening probability or Ca^{2+} permeability of NMDARs.

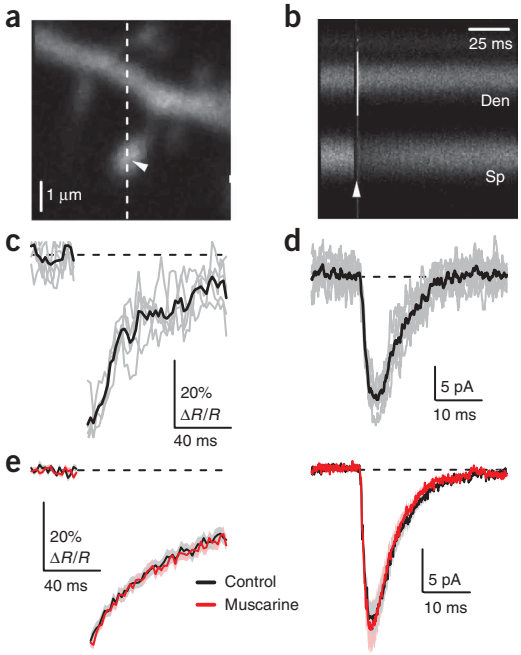

Figure 4 Activation of mAchRs does not modulate AMPAR-mediated currents. (**a**) 2PLSM image of a spiny region from an MSN dendrite filled with 20 μM Alexa-594. (**b**) Red fluorescence in the spine head (Sp) and neighboring dendrite (Den) measured in line scan over the region indicated in **a**. The arrowheads in **a** and **b** indicate the location and timing, respectively, of a 500-μs pulse of 720-nm laser light used to photobleach Alexa-594 fluorescence in the spine head. (**c**) Five consecutive red fluorescence bleaching (~50%) trials (gray) and the corresponding average (black) used to standardize laser power. (**d**) AMPAR-mediated uEPSC evoked by 2PLU of caged glutamate in the presence of the NMDAR antagonist CPP (10 μM) using the laser power determined in **c**. Individual trials (gray traces) and the corresponding average (black trace) are shown. (**e**) Average photobleaching transients (left) and AMPAR mediated uEPSCs (right) measured in control conditions (black, $n = 26$ spines) and in the presence of muscarine (red, $n = 25$ spines). Solid lines indicate the mean and the shaded regions indicate the mean ± s.e.m.

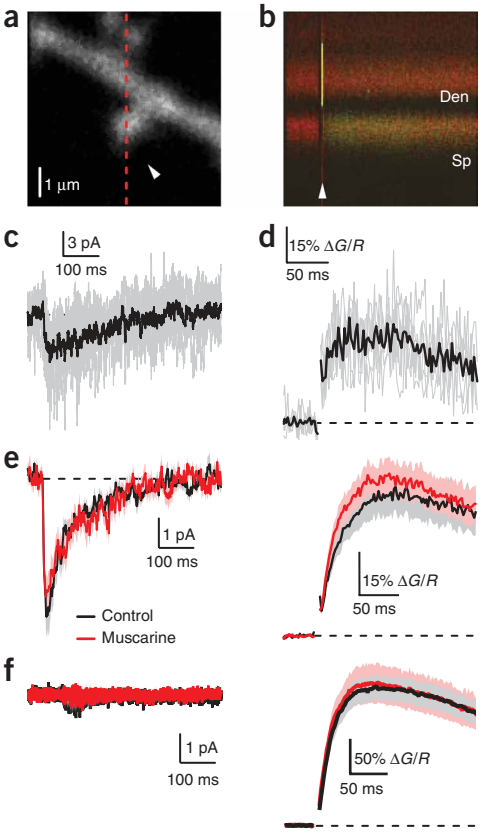

Figure 5 Activation of mAchRs does not modulate NMDAR-mediated currents or Ca^{2+} transients. (**a**) 2PLSM image of a spiny region from an MSN dendrite filled with 20 µM Alexa-594 and 300 µM Fluo-5F. (**b**) Red and green fluorescence in the spine head (Sp) and neighboring dendrite (Den) measured in line scan over the region indicated by the dashed line from **a**. The arrowheads in **a** and **b** indicate the location and timing, respectively, of a 500-µs pulse of 720-nm laser light. The increase in green fluorescence indicates increased intracellular Ca^{2+}. Power was calibrated as described in **Figure 4**. (**c**) NMDAR-mediated uEPSC evoked by glutamate uncaging in the presence of nominally 0 extracellular Mg^{2+} and the AMPAR antagonist NBQX (10 µM). Individual trials (gray traces) and the corresponding average (black trace) are shown. (**d**) NMDAR-mediated Ca^{2+} transients recorded simultaneously with uEPSCs shown in **c**. (**e**) Averages (lines) and averages ± s.e.m. (shaded region) of NMDAR-mediated uEPSCs (left) and spine head Ca transients (right) in control conditions (black, $n = 21$ spines) and in the presence of muscarine (red, $n = 13$ spines). (**f**) Data collected in the same conditions used for optical quantal analysis are presented as in **e**. Each cell was held at the reversal potential for NMDAR-mediated current (~0–10 mV) and in the presence of 1 mM extracellular Mg^{2+}.

Presynaptic control of synaptic potency

Our data indicate that mAchR activation alters synaptic potency without any direct modulation of glutamate receptors. Such effects could arise if synapses exhibit MVR and mAchR activation reduces the number of released vesicles. In this case, other manipulations of presynaptic release probability should also alter potency. We therefore examined the effects of the N-type VGCC blocker ω-Conotoxin GVIA (1.0 µM, Ctx), which is known to reduce the release probability at these synapses[15], using optical quantal analysis (**Fig. 6a**). Similar to muscarine application, Ctx increased the fraction of synaptic failures and reduced the amplitude of Ca^{2+} transients on success trials (**Fig. 6b**). On average ($n = 5$), Ctx application reduced P_s from 0.55 ± 0.12 to 0.30 ± 0.11 ($P < 0.05$) and Pot_{NMDA} from 87.4 ± 8.2% to 57.8 ± 9.2% ($P < 0.05$, **Fig. 6c**). Measurement of 2PLU-evoked Ca^{2+} transients in neurons clamped at 0–10 mV confirmed a lack of postsynaptic effect of Ctx on NMDAR-mediated Ca^{2+}transients (**Fig. 6d**).

To further test whether decreased presynaptic release probability could account for the reduction in synaptic potency, we calculated the relative change in Pot_{NMDA} expected for a change in P_s using a Poisson model of vesicular release (see Online Methods). The observed reductions in Pot_{NMDA} for the muscarine and Ctx experiments were well predicted by the decreases in P_s, yielding an average residual error of 19.4% (**Fig. 6e**). In total, our results indicate that direct manipulation of presynaptic release probability alters synaptic potency in the striatum, which is consistent with a high degree of MVR under basal conditions being reduced by muscarine or Ctx application.

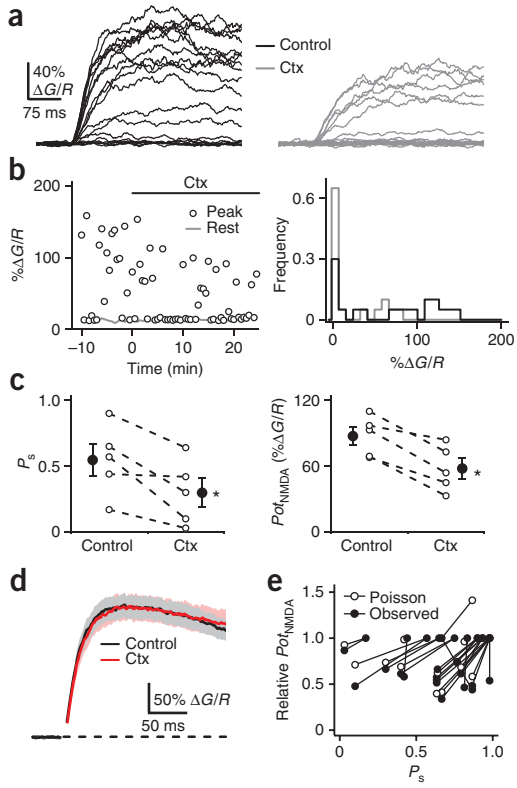

Figure 6 Direct inhibition of vesicular release by blockade of presynaptic N-type Ca^{2+} channels reduces synaptic potency. (**a**) $\Delta G/R$ measured from a single active spine as described in **Figure 3** in control conditions (left) and after bath application of Ctx (1 µM) (right). (**b**) Left, time course of the peak $\Delta G/R$ (circles) and resting fluorescence (gray line) during a baseline period and after application of Ctx. Right, corresponding histogram of $\Delta G/R$ amplitudes in the two conditions. (**c**) Probability of success (P_s, left) and synaptic potency (Pot_{NMDA}, right) for each spine (open circles) under control conditions and after the addition of Ctx. Mean values ± s.e.m. are shown (closed circles). (**d**) Averages (lines) and averages ± s.e.m. (shaded region) of NMDAR-mediated spine head Ca^{2+} transients evoked by glutamate uncaging in control conditions (black, $n = 21$ spines) and in the presence of Ctx (red, $n = 13$ spines). Each cell was voltage clamped at 0–10 mV in the presence of 1 mM extracellular Mg^{2+}. (**e**) Relative synaptic potency (Pot_{NMDA}) before and after muscarine or Ctx application plotted against the corresponding probability of success (P_s). Lines connect values from the same synapse. Closed circles depict the experimental data. Open circles depict the relative potency expected for the observed changes in P_s in a Poisson model of synaptic release (see Online Methods). * indicates a significant difference between groups ($P < 0.05$).

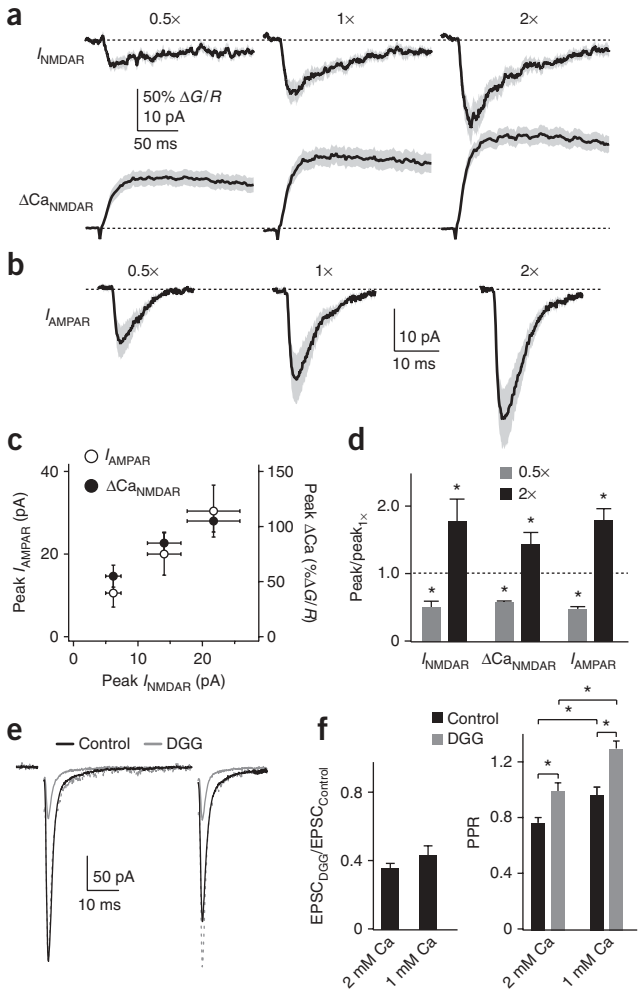

Figure 7 AMPARs and NMDARs are not saturated under basal release conditions. (**a**) NMDAR-mediated uEPSCs (top traces) and Ca^{2+} transients (bottom traces) recorded in the presence of the AMPAR antagonist NBQX (10 μM). Responses were measured using standard laser power (1×), calibrated as described in **Figure 4,** and one-half (0.5×) and twice (2×) the standard power. Solid lines show the average response ($n = 13$ spines), shaded regions are the average response ± s.e.m. (**b**) AMPAR-mediated uEPSCs ($n = 11$ spines) recorded in the presence of the NMDAR antagonist CPP (10 μM). Responses to varying laser power are shown as described in **a**. (**c**) Peak AMPAR-mediated currents and peak NMDAR-mediated currents and Ca transients are directly correlated and vary as a function of laser power. (**d**) AMPAR- and NMDAR-mediated responses are shown for the 0.5× (gray bars) and 2× conditions (black bars), normalized to the 1× amplitude. Peak response amplitudes were significantly reduced and enhanced by decreasing and increasing laser power, respectively ($P < 0.05$). (**e**) AMPAR-mediated EPSCs recorded in the presence of the NMDAR antagonist CPP (10 μM). Responses before (black) and after (gray) application of 2.5 mM γ-DGG are shown. The post–γ-DGG trace is also shown scaled to the baseline amplitude (dashed trace). (**f**) Left, average EPSC peak relative to baseline following γ-DGG application in normal (2 mM) and reduced (1 mM) Ca^{2+}. Right, average PPR before (black) and after (gray) application of γ-DGG under normal and reduced external Ca^{2+}. * indicates a significant difference between conditions ($P < 0.05$), corrected for multiple comparisons in **f**.

Glutamate receptors are not saturated in basal conditions

For postsynaptic receptors to follow changes in the concentration of synaptically released glutamate, AMPARs and NMDARs must not be fully saturated. To examine the degree of receptor saturation, we used 2PLU to stimulate spines with different levels of glutamate. Experiments were performed in the presence of TTX and VGCC antagonists, and laser power was determined as described above (1× condition). Evoked currents were then measured using nominally 0.5×, 1× and 2× laser power (as a result of non-uniform intensity during the 500-μs laser pulse, the actual range of power modulation was less than fourfold). In the presence of NBQX and no extracellular Mg^{2+} ($n = 13$), these three stimuli resulted in NMDAR-mediated uEPSCs of 6.4 ± 1.2 pA, 13.0 ± 2.6 pA and 21.6 ± 4.1 pA, respectively, and Ca^{2+} transients of 58.3 ± 10.6%, 90.1 ± 10.6% and 111.3 ± 10.5%, respectively (**Fig. 7a**). Similar experiments in the presence of CPP ($n = 11$) resulted in non-NMDAR-mediated uEPSCs of 12.5 ± 3.1 pA, 21.1 ± 5.7 pA and 30.3 ± 7.0 pA, respectively (**Fig. 7b**). The currents and Ca^{2+} transients evoked by the 0.5× and 2.0× conditions were significantly different from the 1× condition–evoked responses ($P < 0.05$; **Fig. 7c,d**).

To further study the possibility of receptor saturation, we examined the effect of the low-affinity competitive AMPAR antagonist γ-D-glutamylglycine (γ-DGG) on electrically evoked EPSCs. If receptors are substantially saturated by synaptic activation, decreasing glutamate release by reducing extracellular Ca^{2+} should enhance the current block by γ-DGG. We recorded AMPAR-mediated EPSCs following paired-pulse stimulation in the presence of CPP. Application of γ-DGG in control artificial cerebrospinal fluid (ACSF, 2 mM Ca^{2+}) reduced the amplitudes of the first and second EPSCs and increased PPR (**Fig. 7e**). The increase in PPR is consistent with the relief by γ-DGG of AMPAR desensitization during paired-pulse activation[29]. On average ($n = 13$), γ-DGG significantly reduced the first EPSC to 35.7 ± 2.9% of the control ($P < 0.05$) and increased PPR from 0.77 ± 0.04 to 1.0 ± 0.06 ($P < 0.05$; **Fig. 7f**). Reducing the extracellular Ca^{2+} concentration to 1 mM significantly increased PPR ($P < 0.05$; **Fig. 7f**), indicating a reduction in presynaptic release probability. In 1 mM Ca^{2+}, on average ($n = 7$), γ-DGG reduced the first EPSC to 43.5 ± 5.6% of the control ($P < 0.05$) and increased PPR from 0.97 ± 0.06 to 1.31 ± 0.05 ($P < 0.05$; **Fig. 7f**). The reduction of EPSC amplitude by γ-DGG did not differ between control and low Ca^{2+} conditions, consistent with there being little AMPAR saturation.

Synaptic potency regulates temporal integration

MSNs exhibit voltage-dependent nonlinearities, such as interactions between VGCCs and NMDARs, that enhance the magnitude and summation of synaptic responses[29,30]. We theorized that changes in synaptic potency should influence depolarization in active spines and potentially regulate postsynaptic integration. We therefore re-examined modulation of electrically evoked EPSPs in cells in which the somatic V_m was held constant (**Fig. 8a**). At hyperpolarized potentials ($V_m = -85$ mV), muscarine decreased the EPSP amplitude from 9.5 ± 0.9 mV to 5.0 ± 0.7 mV ($n = 6, P < 0.05$), but did not significantly alter the EPSP width (19.2 ± 1.5 ms versus 18.5 ± 0.9 ms for control and muscarine, respectively; $P > 0.05$, **Fig. 8b**). In cells held at −70 mV, muscarine decreased the average EPSP amplitude from 8.5 ± 0.8 mV to 5.6 ± 1.0 ($n = 6$, $P < 0.05$) and reduced the EPSP width from 32.3 ± 2.3 ms to 25.2 ± 2.5 ms ($P < 0.05$; **Fig. 8b**). These results suggest that changes in synaptic potency can alter response kinetics by influencing postsynaptic voltage-dependent nonlinearities, although this effect may be absent at hyperpolarized potentials as a result of mAchR-mediated closure of inwardly rectifying potassium channels[28].

To further explore this hypothesis, we mimicked a reduction in synaptic potency by co-applying low concentrations of NBQX and CPP. These agents decrease the strength of activation of individual synapses without confounding alteration of postsynaptic membrane properties.

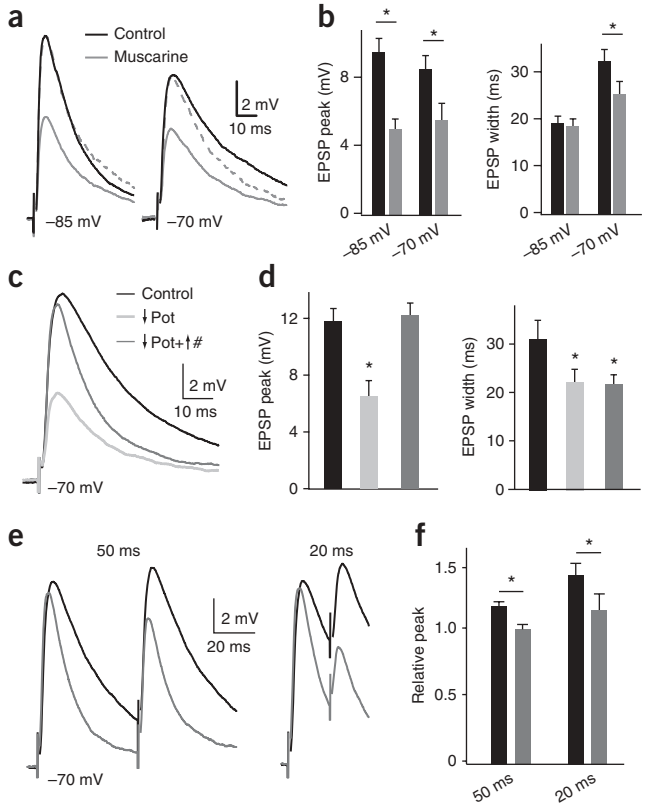

Figure 8 Changes in synaptic potency regulate temporal integration of striatal glutamatergic synapses. (**a**) EPSPs before (black lines) and after (gray lines) muscarine application for two different MSNs in which V_m was held constant at either –85 mV or –70 mV, respectively. The post-muscarine EPSPs scaled to control amplitude are also shown (dashed lines). (**b**) Average EPSP peak amplitude (left) and width (right) in control conditions and after muscarine application for cells held at the indicated V_m. (**c**) EPSPs recorded in an MSN under control conditions (black) after reducing synaptic potency by coapplication of 0.1 μM NBQX and 1.0 μM CPP (↓ Pot, light gray) and after subsequently increasing stimulus intensity to increase the number of synapses activated and return the peak EPSP amplitude to control levels (↓Pot+↑#, medium gray). (**d**) Average EPSP peak amplitude (left) and width (right) in control conditions after reducing synaptic potency and after subsequent increase in the number of activated synapses. Bars are shaded as in **c**. (**e**) Paired EPSPs evoked at either 50-ms (left) or 20-ms (right) intervals recorded in an MSN under control conditions (black lines) or following reduction in synaptic potency and offsetting increase in stimulus intensity (gray lines). (**f**) Average peak amplitude of the second EPSP relative to the first EPSP for 50- and 20-ms intervals, under the same conditions shown in **e**. * indicates a significant difference compared with control conditions ($P < 0.05$).

We determined the concentration of NBQX and CPP necessary to reduce AMPAR and NMDAR currents, respectively, by ~40–50% (the potency decrease seen using optical quantal analysis). In the presence of CPP, application of 0.1 μM NBQX reduced the amplitude of electrically evoked AMPAR-mediated EPSCs from 158.1 ± 12.2 to 91.8 ± 18.0 pA ($n = 6$). In the presence of NBQX, application of 1.0 μM CPP reduced the amplitude of NMDAR-mediated EPSCs (holding potential = 40 mV) from 184.6 ± 22.6 to 106.4 ± 26.9 pA ($n = 4$). These antagonists had no significant effect on the width of either AMPAR-mediated (3.2 ± 0.2 versus 3.6 ± 0.3 ms, $P > 0.05$) or NMDAR-mediated (83.6 ± 7.3 versus 81.0 ± 6.2 ms, $P > 0.05$) EPSCs (control versus drug, respectively).

We next compared EPSPs evoked in control conditions, following co-application of NBQX (0.1 μM) and CPP (1.0 μM), and after increasing stimulus strength in the presence of NBQX and CPP to restore the amplitude of the EPSP to that measured in control conditions (**Fig. 8c**). This tests the hypothesis that changes in synaptic potency and changes in the total number of active synapses have qualitatively different effects on postsynaptic responses. Co-application of NBQX and CPP reduced the EPSP amplitude and width at half-maximal amplitude (**Fig. 8c**). Increasing stimulus intensity returned the amplitude to that seen in control conditions, but did not restore the EPSP width. On average ($n = 8$), decreasing synaptic potency reduced the EPSP amplitude from 11.9 ± 0.9 to 6.6 ± 1.2 mV ($P < 0.05$) and the EPSP width from 31.1 ± 4.2 to 22.3 ± 2.8 ms ($P < 0.05$; **Fig. 8d**). Increasing the total number of active synapses by increasing stimulus intensity restored the EPSP amplitude (12.4 ± 0.9 mV), but failed to restore the EPSP width (21.9 ± 2.2 ms, $P < 0.05$ relative to control), indicating that this parameter is selectively sensitive to the single synapse potency and not to the cumulative multi-synaptic depolarization.

The narrowing of the EPSP following reduction in synaptic potency was sufficient to affect the temporal summation of synaptic potentials during paired simulation (**Fig. 8e**). On average ($n = 7$), under control conditions, the amplitude of the second EPSP relative to that of the first EPSP at 50-ms and 20-ms intervals was 1.16 ± 0.04 and 1.39 ± 0.08, respectively (**Fig. 8f**). Following co-application of NBQX and CPP and an offsetting increase in stimulation strength, the relative amplitudes of the second EPSPs at the two intervals were significantly reduced to 0.99 ± 0.04 ($P < 0.05$) and 1.12 ± 0.13 ($P < 0.05$), respectively. These results demonstrate that modulation of synaptic potency regulates integration independently of changes in the total postsynaptic depolarization.

DISCUSSION

Ach contributes to the regulation of brain function through a diversity of actions[5,36–38]. In the striatum, Ach is released by interneurons that receive inputs from the cortex and thalamus, providing feedforward modulation that is critical for the generation of normal movement and learning in operant conditioning tasks[4,9–11]. We used optical methods to analyze the pre- and postsynaptic effects of mAchR activation. As described previously, we found that Ach acts presynaptically to reduce the probability of glutamate release at excitatory synapses[15–17,19]. We also found that striatal glutamatergic synapses showed a high basal degree of MVR and that cholinergic reduction of release probability decreased the potency of individual synapses by lowering the concentration of glutamate in the synaptic cleft. Decreasing synaptic potency reduced the duration of postsynaptic EPSPs and limited their temporal summation. Our results provide a detailed description of cholinergic actions at a single central synapse and demonstrate a previously unknown mechanism of presynaptic control over post-synaptic integration.

Presynaptic regulation of synaptic potency

Presynaptic terminals of striatal afferent fibers express M2-type mAchRs, the activation of which reduces evoked and spontaneous synaptic responses and increases PPRs (**Fig. 1** and refs. 15–17,19,23). Thus, mAchR activation decreases the release probability, most likely via inhibition of presynaptic P/Q-type VGCCs[15] and reduction of action potential–induced Ca^{2+} increases in the bouton. The post-synaptic actions of mAchR activation are less clear. Previous reports indicate that muscarinic agonists do not alter the response to

iontophoretically applied glutamate[16] or the amplitude of spontaneous synaptic events[23], although one study found that muscarinic agonists enhanced the response to exogenously applied NMDA[24]. However, activation of postsynaptic M1-type mAchRs inhibits N- and L-type VGCCs, as well as multiple potassium conductances[25–28,39,40], and these effects may indirectly modulate glutamate transmission as a result of the voltage dependence of NMDAR opening. Indeed, L-type VGCCs and NMDARs can interact to boost and broaden postsynaptic responses in MSNs[29,30].

Our results indicate that muscarine reduces synaptic potency by decreasing the concentration of released glutamate in the synaptic cleft. We conclude that the most likely explanation is that striatal glutamatergic boutons release multiple vesicles per action potential under basal conditions. Application of muscarine reduces the probability of release, thereby decreasing the number of fusion events and, consequently, the synaptic glutamate concentration. This conclusion is dependent on two assumptions. First, that the Ca^{2+} transient observed in each spine is mediated by glutamate release from a single presynaptic terminal, a position supported by ultrastructural analysis showing that most MSN spines are targeted by a single glutamatergic bouton[13,14]. Second, spillover of glutamate from neighboring synapses does not contribute to measured spine Ca^{2+} transients. In support of this assumption, spine Ca^{2+} imaging is sensitive to the opening of single NMDARs[41], and local electrical stimulation in analyzed experiments did not result in measurable Ca^{2+} transients in neighboring spines. In addition, the VGCC blocker Ctx acutely mimicked the actions of muscarine, arguing strongly that changes in glutamate clearance or vesicle filling are unlikely to explain our results.

Multivesicular release has been observed at a variety of central synapses. Cerebellar parallel fiber–Purkinje cell[42] and hippocampal CA3–CA1 synapses exhibit low basal release probability[31,43,44], but MVR can occur when release is enhanced. In contrast, at retinal bipolar cells to amacrine AII ribbon synapses[45] and climbing fiber inputs to Purkinje cells[46,47], the probability of release and occurrence of MVR is high under basal conditions. Similarly, we found that striatal glutamatergic synapses have a high release probability and a pronounced degree of MVR during basal transmission. The functional consequences of MVR depend on the degree of receptor saturation, which limits the postsynaptic sensitivity to varying glutamate concentration. Using either glutamate uncaging or application of the low-affinity AMPAR antagonist γ-DGG, we found that neither AMPARs nor NMDARs at striatal glutamatergic synapses were saturated, despite the occurrence of MVR.

Functional consequences

The activity of individual MSNs *in vivo* is dependent on the integration of synchronous synaptic inputs arriving predominantly from the cortex[48]. Furthermore, integration in MSNs is inherently nonlinear as a result of engagement of dendritic voltage-dependent conductances and dependence on the spatiotemporal pattern of active synapses[29]. We found that activation of mAchRs narrowed EPSPs. Moreover, mimicking reduced potency with glutamate receptor antagonists also shortened EPSP duration and decreased temporal summation. This effect was not a result of a reduction in the total number of active synapses. One possible explanation is that reduced glutamate per synapse produces less depolarization in individual spines, thus decreasing the activation of voltage-sensitive channels, including L-type VGCCs and NMDARs[29,30].

Our findings differ from those of a previous study showing that mAchR activation increases the duration of EPSPs as a result of a reduction of an inwardly rectifying potassium conductance[28]. However, this earlier study was performed at more hyperpolarized potentials and with NMDARs blocked, preventing the voltage-dependent boosting of EPSP amplitude and duration. Indeed, in our experiments, muscarine did not produce a narrowing of EPSPs recorded at –85 mV. Our results suggest that the release of Ach diminishes the ability of MSNs to respond to synchronized cortical inputs, particularly at relatively depolarized potentials seen *in vivo*. Furthermore, they suggest that other striatal modulators of presynaptic release probability, such as endocannabinoids[49], are also likely to produce postsynaptic changes in EPSP kinetics and temporal integration. Finally, given the changes in release probability that occur across development, determining the contribution of MVR to synaptic transmission and neuromodulation in older animals remains an interesting avenue for future exploration.

METHODS

Methods and any associated references are available in the online version of the paper at http://www.nature.com/natureneuroscience/.

ACKNOWLEDGMENTS

The authors thank members of the Sabatini laboratory, A. Carter, W. Regehr and J. Cardin for helpful comments during the preparation of this manuscript. This work was funded by a Parkinson's Disease Foundation Postdoctoral Fellowship (M.J.H.), a Quan Predoctoral Fellowship and National Institute of Neurological Disorders and Stroke predoctoral National Research Service Award (1 F31 NS049655-01, G.J.S.-L.) and grants from the McKnight Foundation and National Institute of Neurological Disorders and Stroke (NS046579, B.L.S.).

AUTHOR CONTRIBUTIONS

M.J.H., G.J.S.-L. and B.L.S. designed the experiments. M.J.H. and G.J.S.-L. carried out the experiments and analyzed the data. M.J.H. and B.L.S. wrote the manuscript.

Published online at http://www.nature.com/natureneuroscience/.
Reprints and permissions information is available online at http://www.nature.com/reprintsandpermissions/.

1. Shepherd, G.M. *The Synaptic Organization of the Brain* (Oxford University Press, Oxford, 2004).
2. Berton, O. & Nestler, E.J. New approaches to antidepressant drug discovery: beyond monoamines. *Nat. Rev. Neurosci.* **7**, 137–151 (2006).
3. Iversen, S.D. & Iversen, L.L. Dopamine: 50 years in perspective. *Trends Neurosci.* **30**, 188–193 (2007).
4. Pisani, A., Bernardi, G., Ding, J. & Surmeier, D.J. Re-emergence of striatal cholinergic interneurons in movement disorders. *Trends Neurosci.* **30**, 545–553 (2007).
5. Lucas-Meunier, E., Fossier, P., Baux, G. & Amar, M. Cholinergic modulation of the cortical neuronal network. *Pflugers Arch.* **446**, 17–29 (2003).
6. Bolam, J.P., Hanley, J.J., Booth, P.A. & Bevan, M.D. Synaptic organization of the basal ganglia. *J. Anat.* **196**, 527–542 (2000).
7. DeLong, M.R. Primate models of movement disorders of basal ganglia origin. *Trends Neurosci.* **13**, 281–285 (1990).
8. Graybiel, A.M. The basal ganglia. *Curr. Biol.* **10**, R509–R511 (2000).
9. Kaneko, S. *et al.* Synaptic integration mediated by striatal cholinergic interneurons in basal ganglia function. *Science* **289**, 633–637 (2000).
10. Kitabatake, Y., Hikida, T., Watanabe, D., Pastan, I. & Nakanishi, S. Impairment of reward-related learning by cholinergic cell ablation in the striatum. *Proc. Natl. Acad. Sci. USA* **100**, 7965–7970 (2003).
11. Apicella, P. Leading tonically active neurons of the striatum from reward detection to context recognition. *Trends Neurosci.* **30**, 299–306 (2007).
12. Calabresi, P., Centonze, D., Gubellini, P., Pisani, A. & Bernardi, G. Acetylcholine-mediated modulation of striatal function. *Trends Neurosci.* **23**, 120–126 (2000).
13. Kemp, J.M. & Powell, T.P. The termination of fibers from the cerebral cortex and thalamus upon dendritic spines in the caudate nucleus: a study with the Golgi method. *Phil. Trans. R. Soc. Lond. B* **262**, 429–439 (1971).
14. Wilson, C.J. & Groves, P.M. Fine structure and synaptic connections of the common spiny neuron of the rat neostriatum: a study employing intracellular inject of horseradish peroxidase. *J. Comp. Neurol.* **194**, 599–615 (1980).
15. Barral, J., Galarraga, E. & Bargas, J. Muscarinic presynaptic inhibition of neostriatal glutamatergic afferents is mediated by Q-type Ca^{2+} channels. *Brain Res. Bull.* **49**, 285–289 (1999).
16. Malenka, R.C. & Kocsis, J.D. Presynaptic actions of carbachol and adenosine on corticostriatal synaptic transmission studied *in vitro*. *J. Neurosci.* **8**, 3750–3756 (1988).

17. Pakhotin, P. & Bracci, E. Cholinergic interneurons control the excitatory input to the striatum. *J. Neurosci.* **27**, 391–400 (2007).
18. Calabresi, P., Centonze, D., Gubellini, P., Pisani, A. & Bernardi, G. Blockade of M2-like muscarinic receptors enhances long-term potentiation at corticostriatal synapses. *Eur. J. Neurosci.* **10**, 3020–3023 (1998).
19. Sugita, S., Uchimura, N., Jiang, Z.G. & North, R.A. Distinct muscarinic receptors inhibit release of gamma-aminobutyric acid and excitatory amino acids in mammalian brain. *Proc. Natl. Acad. Sci. USA* **88**, 2608–2611 (1991).
20. Aznavour, N., Mechawar, N., Watkins, K.C. & Descarries, L. Fine structural features of the acetylcholine innervation in the developing neostriatum of rat. *J. Comp. Neurol.* **460**, 280–291 (2003).
21. Izzo, P.N. & Bolam, J.P. Cholinergic synaptic input to different parts of spiny striatonigral neurons in the rat. *J. Comp. Neurol.* **269**, 219–234 (1988).
22. Galarraga, E. *et al.* Cholinergic modulation of neostriatal output: a functional antagonism between different types of muscarinic receptors. *J. Neurosci.* **19**, 3629–3638 (1999).
23. Hernández-Echeagaray, E., Galarraga, E. & Bargas, J. 3-Alpha-chloro-imperialine, a potent blocker of cholinergic presynaptic modulation of glutamatergic afferents in the rat neostriatum. *Neuropharmacology* **37**, 1493–1502 (1998).
24. Calabresi, P., Centonze, D., Gubellini, P., Pisani, A. & Bernardi, G. Endogenous ACh enhances striatal NMDA responses via M1-like muscarinic receptors and PKC activation. *Eur. J. Neurosci.* **10**, 2887–2895 (1998).
25. Howe, A.R. & Surmeier, D.J. Muscarinic receptors modulate N-, P- and L-type Ca^{2+} currents in rat striatal neurons through parallel pathways. *J. Neurosci.* **15**, 458–469 (1995).
26. Perez-Rosello, T. *et al.* Cholinergic control of firing pattern and neurotransmission in rat neostriatal projection neurons: role of CaV2.1 and CaV2.2 Ca^{2+} channels. *J. Neurophysiol.* **93**, 2507–2519 (2005).
27. Shen, W., Hamilton, S.E., Nathanson, N.M. & Surmeier, D.J. Cholinergic suppression of KCNQ channel currents enhances excitability of striatal medium spiny neurons. *J. Neurosci.* **25**, 7449–7458 (2005).
28. Shen, W. *et al.* Cholinergic modulation of Kir2 channels selectively elevates dendritic excitability in striatopallidal neurons. *Nat. Neurosci.* **10**, 1458–1466 (2007).
29. Carter, A.G., Soler-Llavina, G.J. & Sabatini, B.L. Timing and location of synaptic inputs determine modes of subthreshold integration in striatal medium spiny neurons. *J. Neurosci.* **27**, 8967–8977 (2007).
30. Liu, J.C. *et al.* Calcium modulates dopamine potentiation of N-methyl-D-aspartate responses: electrophysiological and imaging evidence. *J. Neurosci. Res.* **76**, 315–322 (2004).
31. Oertner, T.G. Sabatini, Nimchinsky & Svoboda. Facilitation at single synapses probed with optical quantal analysis. *Nat. Neurosci.* **5**, 657–664 (2002).
32. Stevens, C.F. & Wang, Y. Facilitation and depression at single central synapses. *Neuron* **14**, 795–802 (1995).
33. Bloodgood, B.L. & Sabatini, B.L. Nonlinear regulation of unitary synaptic signals by CaV(2.3) voltage-sensitive calcium channels located in dendritic spines. *Neuron* **53**, 249–260 (2007).
34. Busetto, G., Higley, M.J. & Sabatini, B.L. Developmental presence and disappearance of postsynaptically silent synapses on dendritic spines of rat layer 2/3 pyramidal neurons. *J. Physiol. (Lond.)* **586**, 1519–1527 (2008).
35. Carter, A.G. & Sabatini, B.L. State-dependent calcium signaling in dendritic spines of striatal medium spiny neurons. *Neuron* **44**, 483–493 (2004).
36. Hasselmo, M.E. The role of acetylcholine in learning and memory. *Curr. Opin. Neurobiol.* **16**, 710–715 (2006).
37. Jones, B.E. Activity, modulation and role of basal forebrain cholinergic neurons innervating the cerebral cortex. *Prog. Brain Res.* **145**, 157–169 (2004).
38. McCormick, D.A. Actions of acetylcholine in the cerebral cortex and thalamus and implications for function. *Prog. Brain Res.* **98**, 303–308 (1993).
39. Akins, P.T., Surmeier, D.J. & Kitai, S.T. Muscarinic modulation of a transient K^+ conductance in rat neostriatal neurons. *Nature* **344**, 240–242 (1990).
40. Olson, P.A. *et al.* G-protein-coupled receptor modulation of striatal CaV1.3 L-type Ca^{2+} channels is dependent on a Shank-binding domain. *J. Neurosci.* **25**, 1050–1062 (2005).
41. Nimchinsky, E.A., Yasuda, R., Oertner, T.G. & Svoboda, K. The number of glutamate receptors opened by synaptic stimulation in single hippocampal spines. *J. Neurosci.* **24**, 2054–2064 (2004).
42. Foster, K.A., Crowley, J.J. & Regehr, W.G. The influence of multivesicular release and postsynaptic receptor saturation on transmission at granule cell to Purkinje cell synapses. *J. Neurosci.* **25**, 11655–11665 (2005).
43. Christie, J.M. & Jahr, C.E. Multivesicular release at Schaffer collateral–CA1 hippocampal synapses. *J. Neurosci.* **26**, 210–216 (2006).
44. Tong, G. & Jahr, C.E. Multivesicular release from excitatory synapses of cultured hippocampal neurons. *Neuron* **12**, 51–59 (1994).
45. Singer, J.H., Lassova, L., Vardi, N. & Diamond, J.S. Coordinated multivesicular release at a mammalian ribbon synapse. *Nat. Neurosci.* **7**, 826–833 (2004).
46. Foster, K.A., Kreitzer, A.C. & Regehr, W.G. Interaction of postsynaptic receptor saturation with presynaptic mechanisms produces a reliable synapse. *Neuron* **36**, 1115–1126 (2002).
47. Wadiche, J.I. & Jahr, C.E. Multivesicular release at climbing fiber-Purkinje cell synapses. *Neuron* **32**, 301–313 (2001).
48. Wilson, C.J. & Kawaguchi, Y. The origins of two-state spontaneous membrane potential fluctuations of neostriatal spiny neurons. *J. Neurosci.* **16**, 2397–2410 (1996).
49. Adermark, L. & Lovinger, D.M. Frequency-dependent inversion of net striatal output by endocannabinoid-dependent plasticity at different synaptic inputs. *J. Neurosci.* **29**, 1375–1380 (2009).

ONLINE METHODS

Slice preparation and pharmacology. All animal handling was performed in accordance with guidelines approved by the Harvard Institutional Animal Care and Use Committee and federal guidelines. Recordings were made from MSNs in striatal slices taken from postnatal day 15–18 Sprague-Dawley rats. Sagittal (**Fig. 8**) or coronal (**Figs. 1–7**) slices (300 μm thick) were cut in ice-cold external solution containing 110 mM choline, 25 mM $NaHCO_3$, 1.25 mM NaH_2PO_4, 2.5 mM KCl, 7 mM $MgCl_2$, 0.5 mM $CaCl_2$, 25 mM glucose, 11.6 mM sodium ascorbate and 3.1 mM sodium pyruvate, bubbled with 95% O_2 and 5% CO_2. Slices were then transferred to ACSF containing 127 mM NaCl, 25 mM $NaHCO_3$, 1.25 mM NaH_2PO_4, 2.5 mM KCl, 1 mM $MgCl_2$, 2 mM $CaCl_2$ and 25 mM glucose, bubbled with 95% O_2 and 5% CO_2. After an incubation period of 30–40 min at 34 °C, the slices were stored at 22–25 °C. All experiments were conducted at 32 °C. In all experiments, 50 μM picrotoxin was present in the ACSF to block $GABA_{A/C}$ receptor–mediated inhibition. For all glutamate uncaging experiments, 10 μM serine was included in the ACSF to reduce NMDAR desensitization and VGCCs were blocked with a cocktail of 1 μM ω-conotoxin-MVIIC (N/P/Q types), 20 μM nimodipine (L types) and 10 μM mibefradil (R and T types). For some experiments, extracellular $MgCl_2$ was nominally reduced to 0 μM. In experiments in which extracellular Ca^{2+} was reduced to 1 mM, Mg^{2+} was increased to 2 mM to maintain a constant concentration of divalent ions. Finally, in some experiments, one or more of the following drugs were added to the ACSF, unless otherwise stated, at the following concentrations 10 μM muscarine, 10 μM NBQX, 10 μM CPP, 50 μM AP5, 1 μM TTX, 1 μM ω-conotoxin-GVIA or 2500 μM γ-DGG. To block ~50% of AMPARs and NMDARs (**Fig. 8**), 0.1 and 1 μM of NBQX and CPP were used, respectively. All chemicals were from Sigma or Tocris, with the exception of ω-conotoxin-GVIA and ω-conotoxin-MVIIC (Peptides International).

Electrophysiology and imaging. Whole-cell recordings were obtained from MSNs identified with infrared differential interference contrast videomicroscopy and 2PLSM on the basis of their small cell bodies and prominent dendritic spines. For current-clamp recordings, glass electrodes (2–4 MΩ) were filled with internal solution containing 135 mM $KMeSO_3$, 10 mM HEPES, 4 mM $MgCl_2$, 4 mM Na_2ATP, 0.4 mM NaGTP and 10 mM sodium creatine phosphate, adjusted to pH 7.4 with KOH. For voltage-clamp recordings, cesium was substituted for potassium to improve space clamping. For physiology-only experiments, 1 mM EGTA and 20 μM Alexa Fluor-594 (to image neuronal morphology) were added to the internal solution. For Ca^{2+}-imaging experiments, 300 μM of the Ca^{2+}-sensitive indicator Fluo-5F and 20 μM Alexa Fluor-594 were added. Current and voltage recordings were made using a Multiclamp 700B amplifier. Data was filtered at 5 kHz and digitized at 10 kHz. Excitatory input fibers were stimulated with a small glass electrode (tip diameter, 2–4 μm) filled with ACSF using brief (0.2 ms) current injections. For paired-pulse stimulation experiments, the electrode was placed at the border between the striatum and the overlying white matter. For optical quantal analysis experiments, the electrode was placed ~10 μm from the dendritic spine of interest.

Intracellular Ca^{2+} imaging and glutamate uncaging were accomplished with a custom microscope combining 2PLSM and 2PLU, as previously described[33,35]. Neurons were filled via the patch electrode for 10–15 min before imaging. Fluo-5F (green) and Alexa Fluor-594 (red) were excited using 840-nm light to monitor Ca^{2+} signals and spine morphology, respectively. To measure Ca^{2+} signals, we collected green and red fluorescence during 500-Hz line scans across a spine and a neighboring dendrite. Ca^{2+} signals were quantified as increases in green fluorescence from baseline normalized to the red fluorescence ($\Delta G/R$). Reference frame scans were taken between each acquisition to correct for small spatial drift of the preparation over time.

For 2PLU experiments, MNI-glutamate was bath applied at 2.5 mM, and glutamate uncaging was achieved using a 0.5-ms pulse of 720-nm light. To achieve standard uncaging power, (which translates into a constant amount of glutamate uncaged on each trial) we used photobleaching of Alexa Fluo-594 in the spine of interest as previously described[33]. Bleaching is a function of the laser power and thus provides readout of power delivery that is independent of spine depth and electrophysiological responses.

Data acquisition and analysis. Imaging and physiology data were acquired using National Instruments boards and custom software written in MATLAB (Mathworks)[50]. Off-line analysis was performed using custom routines written in MATLAB and Igor Pro (Wavemetrics). Peak amplitudes of electrically evoked EPSPs were calculated by averaging a 3-ms window around the peak. The amplitudes of electrically evoked EPSCs and uncaging-evoked EPSCs mediated by AMPARs were calculated by averaging over a 2-ms window, whereas a 10-ms window was used to calculate peaks of NMDAR-mediated EPSCs. EPSP and EPSC widths were calculated as the interval between points at half-maximal amplitude. For imaging experiments, measurements of $\Delta G/R$ were calculated by taking the average of the signal over a 150-ms post-stimulus window.

For paired-pulse experiments, we measured the response to a single stimulation or paired stimulation at an interstimulus interval of 50 or 20 ms. The PPR was calculated by subtracting the response to the single stimulus from the response to the paired stimulus and then calculating the ratio of the peak of the remaining response to the single response.

For optical quantal analysis, successes were distinguished from failures by setting a threshold equal to two s.d. above baseline noise. To determine the effect of muscarine and Ctx on the amplitude of NMDAR-mediated Ca^{2+} signals, we compared the average $\Delta G/R$ on success trials during the baseline period with the average $\Delta G/R$ after application of each drug. The probability of success was calculated by dividing the number of successful trials by the total number of trials during either baseline or after bath application of each drug. To ensure that the dendrite was not stimulated directly, we limited our analysis to those experiments in which Ca^{2+} entry was confined to a single spine.

In sections describing optical or uncaging responses measured from individual spines, the stated n indicates the number of spines analyzed. In sections describing electrically evoked synaptic responses, the stated n indicates the number of cells analyzed. All statistics are expressed as mean ± s.e.m. and comparisons were made using a two-tailed Student's t test. Differences were judged to be statistically significant for $P < 0.05$.

Poisson model. To test whether reduced probability of vesicle release could adequately explain the observed changes in postsynaptic potency, we developed a Poisson model of synaptic transmission that assumes independent release of multiple docked vesicles per active zone. In this model, the probability of release of x vesicles following an action potential is given by a function of a single parameter λ that is the average number of released vesicles (that is, $\lambda = <x>$), such that:

$$P(x) = \frac{\lambda^x e^{-\lambda}}{x!}$$

Therefore, the probability of release of one or more vesicles (that is, P_s, the probability of seeing a synaptic response on any given trial) is related to λ by

$$\lambda = -\ln(P(0)) = -\ln(1 - P_s)$$

Assuming a linear relationship between the number of released vesicles and the degree of NMDAR activation, the mean spine head Ca^{2+} transient amplitude (averaged across all trials including successes and failures) is given by $\left\langle \frac{\Delta G}{R} \right\rangle = \lambda q$, where q is the quantal postsynaptic amplitude for a single vesicle. Furthermore, the mean spine head Ca^{2+} transient amplitude of only success trials (the synaptic potency, Pot_{NMDA}) is

$$Pot_{NMDA} = \frac{\lambda q}{P_s} = -\ln(1 - P_s)\frac{q}{P_s}$$

If the quantal amplitude q is the same in two conditions (that is, before and after drug application), the ratio of synaptic potencies in the two conditions is purely a function of the probability of successful vesicular release

$$\frac{Pot_1}{Pot_2} = \frac{\frac{\ln(1-P_{s1})}{P_{s1}}}{\frac{\ln(1-P_{s2})}{P_{s2}}} \quad (1)$$

Figure 6e shows the results of using this equation to predict changes in synaptic potency for all experiments involving either muscarine or Ctx application. We plotted the expected fractional change in Pot_{NMDA} as a function of the observed change in P_s. The model ignores possible supralinearities in the activation of NMDARs as a result of a Hill coefficient of greater than 1 for activation by glutamate and possible sublinearities resulting from saturation of Ca^{2+} indicator. Despite these simplifications and the lack of free parameters, Equation (1) fits the experimental data with a residual error of $<20\%$.

50. Pologruto, T.A., Sabatini, B.L. & Svoboda, K. ScanImage: flexible software for operating laser-scanning microscopes. *Biomed. Eng. Online* **2**, 13 (2003).

doi:10.1038/nn.2368